

2011

## Magnetic and ferroelectric properties of multiferroic Bi<sub>2</sub>NiMnO<sub>6</sub> nanoparticles

Yi Du

*University of Wollongong, ydu@uow.edu.au*

Zhenxiang Cheng

*University of Wollongong, cheng@uow.edu.au*

Xiaolin Wang

*University of Wollongong, xiaolin@uow.edu.au*

Peng Liu

*pl990@uowmail.edu.au*

S. X. Dou

*University of Wollongong, shi@uow.edu.au*

Follow this and additional works at: <https://ro.uow.edu.au/engpapers>



Part of the [Engineering Commons](#)

<https://ro.uow.edu.au/engpapers/2922>

---

### Recommended Citation

Du, Yi; Cheng, Zhenxiang; Wang, Xiaolin; Liu, Peng; and Dou, S. X.: Magnetic and ferroelectric properties of multiferroic Bi<sub>2</sub>NiMnO<sub>6</sub> nanoparticles 2011, 07B507-1-07B507-3.  
<https://ro.uow.edu.au/engpapers/2922>

## Magnetic and ferroelectric properties of multiferroic Bi<sub>2</sub>NiMnO<sub>6</sub> nanoparticles

Y. Du, Z. X. Cheng, X. L. Wang, P. Liu, and S. X. Dou

Citation: *J. Appl. Phys.* **109**, 07B507 (2011); doi: 10.1063/1.3537943

View online: <http://dx.doi.org/10.1063/1.3537943>

View Table of Contents: <http://jap.aip.org/resource/1/JAPIAU/v109/i7>

Published by the American Institute of Physics.

---

### Related Articles

Thermally activated magnetization switching in a nanostructured synthetic ferrimagnet

*J. Appl. Phys.* **113**, 063914 (2013)

Probing nanowire edge roughness using an extended magnetic domain wall

*Appl. Phys. Lett.* **102**, 062409 (2013)

Reversal process of a magnetic vortex core under the combined action of a perpendicular field and spin transfer torque

*Appl. Phys. Lett.* **102**, 062401 (2013)

Stripe-vortex transitions in ultrathin magnetic nanostructures

*J. Appl. Phys.* **113**, 054312 (2013)

Phase locking of vortex-based spin-torque nanocontact oscillators by antivortices

*Appl. Phys. Lett.* **102**, 052403 (2013)

---

### Additional information on J. Appl. Phys.

Journal Homepage: <http://jap.aip.org/>

Journal Information: [http://jap.aip.org/about/about\\_the\\_journal](http://jap.aip.org/about/about_the_journal)

Top downloads: [http://jap.aip.org/features/most\\_downloaded](http://jap.aip.org/features/most_downloaded)

Information for Authors: <http://jap.aip.org/authors>

## ADVERTISEMENT



The advertisement banner features a green and white background with abstract, flowing lines. On the left, the text "AIP Advances" is displayed in a stylized font, with "AIP" in blue and "Advances" in green. To the right of the text is a circular seal with the text "Now Indexed in Thomson Reuters Databases". Below the main text, there is a blue horizontal bar containing the text "Explore AIP's open access journal:". To the right of this bar is a list of three bullet points: "Rapid publication", "Article-level metrics", and "Post-publication rating and commenting".

## Magnetic and ferroelectric properties of multiferroic $\text{Bi}_2\text{NiMnO}_6$ nanoparticles

Y. Du, Z. X. Cheng, X. L. Wang,<sup>a)</sup> P. Liu, and S. X. Dou

*Institute for Superconducting and Electronic Materials, University of Wollongong, Wollongong, New South Wales 2522, Australia*

(Presented 15 November 2010; received 22 September 2010; accepted 22 October 2010; published online 21 March 2011)

Multiferroic  $\text{Bi}_2\text{NiMnO}_6$  nanoparticles were synthesized by a simple electrospray method.  $\text{Bi}_2\text{NiMnO}_6$  nanoparticles crystallize in the monoclinic structure with space group  $C121$ . The particles show a uniform spherical shape with a diameter of 100 nm to 300 nm. The ferromagnetic transition of  $\text{Bi}_2\text{NiMnO}_6$  is confirmed at 122 K. The room temperature ferroelectricity of the  $\text{Bi}_2\text{NiMnO}_6$  nanoparticles is verified by Kelvin probe force microscopy. © 2011 American Institute of Physics. [doi:10.1063/1.3537943]

### I. INTRODUCTION

Multiferroic materials, which show coexistence of ferroelectric and magnetic orderings, have been attracting intense interest due to their interesting fundamental nature and potentially wide applications.<sup>1–3</sup> However, candidate multiferroic materials are very rare because ferromagnetism requires transition metals with unpaired 3d electrons and an unfilled 3d orbital, while ferroelectricity needs transition metals with filled 3d orbitals. Oxide perovskites ( $\text{ABO}_3$ ) have been proposed as potential multiferroic materials with possible A-site ferroelectricity and B-site magnetism. Even though  $\text{ABO}_3$  compounds, such as  $\text{BiFeO}_3$ ,<sup>4</sup>  $\text{BiMnO}_3$ ,<sup>5</sup> and  $\text{DyFeO}_3$ ,<sup>6</sup> have demonstrated coupling between the magnetic and ferroelectric orderings, they are characterized by serious current leakage problems or weak magnetoelectric coupling, which makes them very difficult to incorporate into applications. Recently, double-perovskite multiferroic compounds ( $A_2BB'O_6$ ), such as  $\text{Bi}_2\text{FeMnO}_6$ ,<sup>7</sup>  $\text{Bi}_2\text{FeCrO}_6$ ,<sup>8</sup> and  $\text{Bi}_2\text{NiMnO}_6$ ,<sup>9</sup> have been theoretically designed. In these double-perovskite oxides, Bi cations with lone pair  $s^2$  electrons occupy the A sites, while two transition metal atoms occupy the B and B' sites, alternatively. In previous studies, room temperature multiferroic properties were observed in  $\text{Bi}_2\text{FeMnO}_6/\text{Nd:BiFeO}_3$  bilayered films.<sup>10</sup> The strong coupling of magnetism and ferroelectricity was confirmed in a  $\text{Bi}_2\text{NiMnO}_6$  thin film sample.<sup>11</sup> However, the ferromagnetic transition of the  $\text{Bi}_2\text{NiMnO}_6$  was not determined due to the large diamagnetic contribution from the  $\text{SrTiO}_3$  substrate. Moreover, to date, little if any effort has been expended on research associated with the nanostructure of these double-perovskite compounds due to the difficulty in synthesis, which usually needs extremely high pressure and high temperature. The intrinsic magnetic interactions and ferroelectric behaviors of these compounds on the nanoscale are unclear, as yet. Investigations focused on developing advanced structural formulations such as zero-, one-, and two-dimensional (0-D, 1-D, and 2-D) nanostructures of double-perovskite multiferroic materials and studies of their physical properties are still desirable.

In this work, nanosized  $\text{Bi}_2\text{NiMnO}_6$  particles have been successfully fabricated by an electrospray method. The structure, morphology, magnetic properties, and ferroelectric properties have all been investigated. The ferromagnetic transition temperature has been determined as 122 K. Switchable polarizations of the  $\text{Bi}_2\text{NiMnO}_6$  nanoparticles were also observed.

### II. EXPERIMENTAL PROCEDURES

$\text{Bi}_2\text{NiMnO}_6$  nanoparticles were synthesized by an electrospray method in a high voltage field (up to 20 kV). Stoichiometric  $\text{Bi}(\text{NO}_3)_3 \cdot 5\text{H}_2\text{O}$  (99.5%, Sigma-Aldrich),  $\text{Mn}(\text{CH}_3\text{COOH})_2 \cdot 5\text{H}_2\text{O}$ , and  $\text{Ni}(\text{NO}_3)_2 \cdot 3\text{H}_2\text{O}$  were dissolved in 200 ml 2-methoxyethanol (Sigma-Aldrich) forming a 0.005 M clear solution. 0.003 M  $\text{NH}_4\text{OH}$  was slowly added to the solution, resulting in a dark brown sol-gel. Then, the precursor was sprayed onto an Si wafer substrate at a temperature of 573 K in an electric field of 16 kV for 2 hours. The as-prepared sample was annealed at 973 K in Ar for 1 hour.

The crystal structure of the samples was examined by X-ray diffraction (XRD; GBC MMA), using Cu-K $\alpha$  radiation at  $\lambda = 1.54056 \text{ \AA}$ , operating at 40 kV voltage and 25 mA current. Field-emission scanning electron microscope (SEM) images were obtained, and X-ray energy dispersive spectroscopy (EDS) analysis was conducted using a JEOL-7500 microscope equipped with EDS. Transmission electron microscope (TEM) images were collected on a JEOL-2100 with an acceleration voltage of 200 kV. The magnetic measurements were carried out using a 14 T physical property measurement system (Quantum Design) over a wide temperature range from 5 K to 300 K. The ferroelectricity of the samples was measured by Kelvin probe force microscopy [(KPFM), Asylum Research MFP-3D], using both contact and noncontact modes.

### III. RESULTS AND DISCUSSION

Figure 1 shows the XRD pattern for the  $\text{Bi}_2\text{NiMnO}_6$  nanoparticles. It indicates that the  $\text{Bi}_2\text{NiMnO}_6$  nanoparticles have crystallized in the monoclinic structure with space group  $C121$ . The lattice parameters are  $a = 9.527 \text{ \AA}$ ,

<sup>a)</sup> Author to whom correspondence should be addressed. Electronic mail: xiaolin@uow.edu.au.

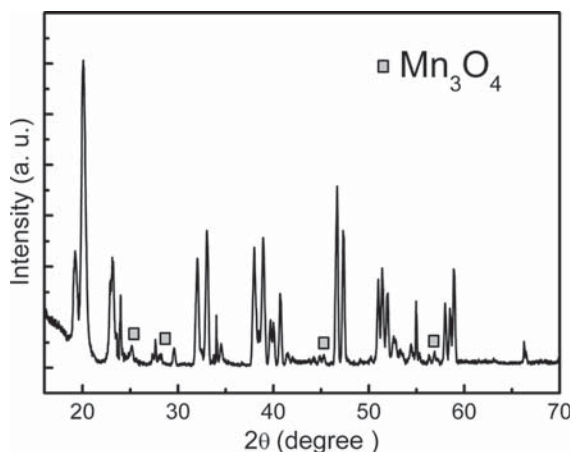


FIG. 1. XRD pattern of  $\text{Bi}_2\text{NiMnO}_6$  nanoparticles fabricated by the electro-spray method.

$b = 5.431 \text{ \AA}$ , and  $c = 9.552 \text{ \AA}$ . The sharp peaks confirm the highly crystalline nature of the as-obtained sample. The impurity peaks are attributed to a small amount of  $\text{Mn}_3\text{O}_4$ .

Figure 2 shows SEM and TEM images of the as-prepared  $\text{Bi}_2\text{NiMnO}_6$  nanoparticles. Clearly, the product consists of a high yield of spherical  $\text{Bi}_2\text{NiMnO}_6$  nanoparticles. The size of the nanoparticles ranges from 100 nm to 350 nm. Because the charged droplets are self-dispersing in the electric field during the electro-spraying process, all of the particles are dispersed without any agglomeration. A magnified SEM image of dispersed  $\text{Bi}_2\text{NiMnO}_6$  nanoparticles is shown as the inset in Fig. 2(a). The nature of the products was also determined by energy dispersive spectroscopy (EDS) analysis. The EDS results confirmed that the as-obtained products contain Bi, Mn, and Ni with an atomic Bi: Mn: Ni ratio of  $\sim 2: 1: 1$ , which agrees with the expected stoichiometry and XRD results. TEM was used to further confirm the morphology and structure of the  $\text{Bi}_2\text{NiMnO}_6$  nanoparticles, as shown in Fig. 2(b). A magnified TEM image of an individual  $\text{Bi}_2\text{NiMnO}_6$  nanoparticle is shown as the inset in Fig. 2(b). The formation mechanism can be explained by the Ostwald ripening model. Initially, the  $\text{Bi}_2\text{NiMnO}_6$  sol is electro-sprayed to form self-dispersing charged droplets in a high-voltage electric field. The solvent will evaporate from the precursor once the droplets become attached to the heated substrate. Then, the nucleation and growth of the  $\text{Bi}_2\text{NiMnO}_6$  particles take place. Some fragment-like dots

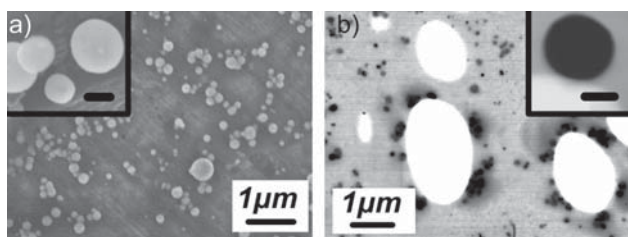


FIG. 2. (a) SEM image of as-prepared  $\text{Bi}_2\text{NiMnO}_6$  nanoparticles. The inset shows a magnified view of the dispersed particles, on which some fragment-like dots are observed. (b) TEM image of  $\text{Bi}_2\text{NiMnO}_6$  nanoparticles; the inset is a magnified view of an individual nanoparticle. The scale bars in both insets represent 100 nm.

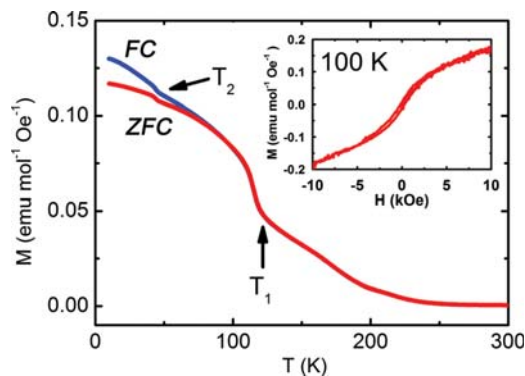


FIG. 3. (Color online) Magnetization as a function of temperature for  $\text{Bi}_2\text{NiMnO}_6$  nanoparticles measured in the temperature range from 5 K to 300 K in a magnetic field of 100 Oe; the inset is the M-H loop measured at 100 K.

are formed on the nanoparticles [see inset in Fig. 2(a)]. Because the system tries to lower its overall energy, the dots on the surface will diffuse into the particles.

Figure 3 shows the magnetization ( $M$ ) as a function of temperature ( $T$ ) for  $\text{Bi}_2\text{NiMnO}_6$  nanoparticles measured in the temperature range from 5 K to 300 K in a magnetic field of 100 Oe. Both zero-field-cooling and field-cooling measurements were conducted. The magnetic contribution from the substrate has been subtracted from the data. Two magnetic transitions were observed at  $T_1 = 122 \text{ K}$  and  $T_2 = 44 \text{ K}$ . In a previous study, it was reported that  $\text{Mn}_3\text{O}_4$  undergoes a ferrimagnetic transition at  $\sim 42 \text{ K}$ .<sup>12</sup> In our sample, the impurity  $\text{Mn}_3\text{O}_4$  was detected in the XRD pattern. Therefore, the magnetic transition at  $T_2$  should be attributed to  $\text{Mn}_3\text{O}_4$  ferrimagnetic ordering. For  $\text{Bi}_2\text{NiMnO}_6$ , it is expected that Ni ions present a valence of +2 with  $e_g$  electrons, while Mn ions present a valence of +4 with no  $e_g$  electrons. According to the Goodenough-Kanamori rules,<sup>13</sup> the expectation for magnetic interaction between  $\text{Ni}^{2+}$  and  $\text{Mn}^{4+}$  should be ferromagnetic ordering with a linear arrangement of Ni-O-Mn. It is believed that  $T_1$  observed in the M-T curve corresponds to the ferromagnetic transition temperature of  $\text{Bi}_2\text{NiMnO}_6$ . To further confirm the aforementioned analysis, the magnetization as a function of magnetic field ( $H$ ) for  $\text{Bi}_2\text{NiMnO}_6$  nanoparticles was measured in a magnetic field of 10 kOe at 100 K, as shown in the Fig. 3 inset. The hysteresis in the M-H loop should only be contributed by  $\text{Bi}_2\text{NiMnO}_6$  at 100 K because it is far higher than the  $\text{Mn}_3\text{O}_4$  ordering temperature. Clear hysteresis behavior has been observed. The coercive field is found to be 190 Oe.

The room temperature ferroelectricity of the  $\text{Bi}_2\text{NiMnO}_6$  nanoparticles was then confirmed by KPFM measurements. To induce the ferroelectric dipoles (poling process), atomic force microscope (AFM) scans were carried out on a sample area of  $1.5 \times 1.5 \mu\text{m}^2$  (scan speed of 19.6 Hz, 512 lines) in contact mode with the given biases of 0 V, 1 V, 3 V, and 5 V. Then, a second AFM scan of the  $1.5 \times 1.5 \mu\text{m}^2$  area (scan speed of 19.6 Hz, 512 lines) with a grounded tip was performed on the same area to discharge the screening charge, which had accumulated during the poling process. Due to a reduction of the screening charge by the discharge process, the surface potential directly indicates the ferroelectric

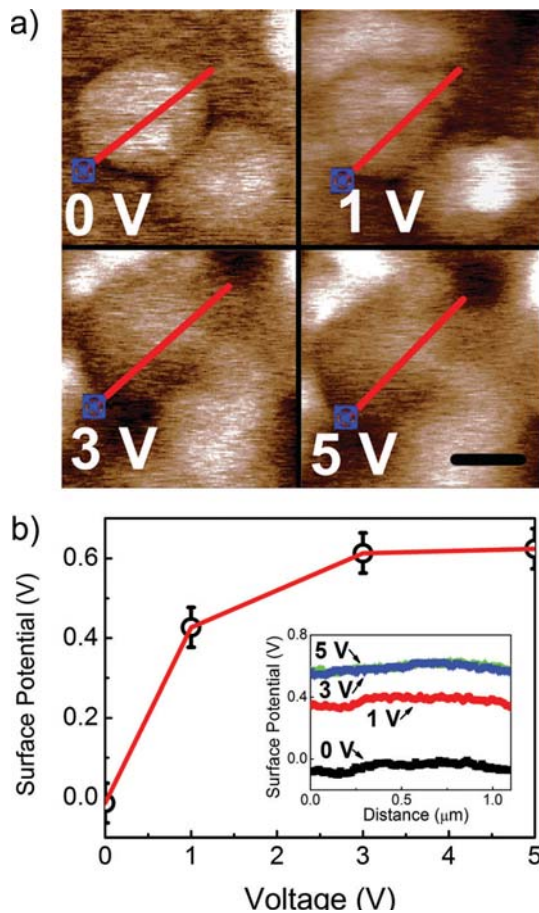


FIG. 4. (Color online) KPFM images of Bi<sub>2</sub>NiMnO<sub>6</sub> nanoparticles: (a) Surface potential images of the sample with the given biases of 0 V, 1.0 V, 3.0 V, and 5.0 V. (b) The sample surface potential as a function of the bias voltage; the inset contains the line potential profiles of the KPFM images of an individual nanoparticle [corresponding to the red lines in Fig. 4(a)]. The scale bar represents 0.5 μm.

polarization charge distribution. Figure 4(a) shows surface potential images of Bi<sub>2</sub>NiMnO<sub>6</sub> nanoparticles with various bias voltages. The polarized particles are brighter than the Si substrate due to their higher potential. The potential line profiles of corresponding individual Bi<sub>2</sub>NiMnO<sub>6</sub> particles in Fig. 4(a) are shown in the inset of Fig. 4(b). Results indicate that the surface potential of Bi<sub>2</sub>NiMnO<sub>6</sub> particles gradually increases when the applied bias voltage increases from 0.5 V to 5 V. The surface potential as a function of bias voltage for the Bi<sub>2</sub>NiMnO<sub>6</sub> nanoparticles is plotted in Fig. 4(b). A non-linear increase in the surface potential induced by the polarizing voltage is observed, which displays a switchable polarization behavior. The surface potential is saturated when

the polarizing voltage is increased up to 3 V. The electric field for the saturation polarization is calculated to be about 600 kV/cm, which is much smaller than that of the Bi<sub>2</sub>NiMnO<sub>6</sub> thin film samples,<sup>14</sup> indicating that the electric dipole can be easily switched in the nanoparticles under low electric field.

#### IV. CONCLUSION

Bi<sub>2</sub>NiMnO<sub>6</sub> nanoparticles have been synthesized by a simple electrospray method. It is found that Bi<sub>2</sub>NiMnO<sub>6</sub> nanoparticles crystallize in the monoclinic structure with space group *C121*. The self-dispersed nanoparticles show a spherical shape with a diameter of 100 nm to 300 nm. The ferromagnetic transition of Bi<sub>2</sub>NiMnO<sub>6</sub> is confirmed at 122 K in the M-T curve. A coercive field of 190 Oe has been observed in the M-H loop. The room temperature ferroelectricity of the Bi<sub>2</sub>NiMnO<sub>6</sub> nanoparticles has been investigated using KPFM by applying bias from 0 V to 5 V.

#### ACKNOWLEDGMENTS

The authors thank the Australian Research Council for providing funding support for this work (DP0987190, DP0558753, and FT 0990287). The authors also thank Dr. Z. P. Guo and Mr. Kouk Hau Seng for their help in sample preparation.

<sup>1</sup>H. Schmid, *Ferroelectrics* **162**, 317 (1994).

<sup>2</sup>N. Hur, S. Park, P. A. Sharma, J. S. Ahn, S. Guha, and S-W. Cheong, *Nature* **429**, 392 (2004).

<sup>3</sup>N. Ikeda, H. Ohsumi, K. Ohwada, K. Ishii, T. Inami, K. Kakurai, Y. Murakami, K. Yoshii, S. Mori, Y. Horibe, and H. Kitô, *Nature* **436**, 1136 (2005).

<sup>4</sup>Z. X. Cheng, X. L. Wang, S. X. Dou, K. Ozawa, and H. Kimura, *Phys. Rev. B* **77**, 092101 (2008).

<sup>5</sup>T. Kimura, S. Kawamoto, I. Yamada, M. Azuma, M. Takano, and Y. Tokura, *Phys. Rev. B* **67**, 180401(R) (2003).

<sup>6</sup>Y. Tokunaga, S. Iguchi, T. Arima, and Y. Tokura, *Phys. Rev. Lett.* **101**, 097205 (2008).

<sup>7</sup>L. Bi, A. R. Taussig, H. Kim, L. Wang, G. F. Dionne, D. Bono, K. Persson, G. D. Ceder, and C. A. Ross, *Phys. Rev. B* **78**, 104106 (2008).

<sup>8</sup>P. Baettig, C. Ederer, and N. A. Spaldin, *Phys. Rev. B* **72**, 214105 (2005).

<sup>9</sup>M. Azuma, K. Takata, T. Saito, S. Ishiwata, Y. Shimakawa, and M. Takano, *J. Am. Chem. Soc.* **127**, 8889 (2005).

<sup>10</sup>H. Zhao, H. Kimura, Z. Cheng, X. Wang, and T. Nishida, *Appl. Phys. Lett.* **95**, 232904 (2009).

<sup>11</sup>P. Padhan, P. LeClair, A. Gupta, and G. Srinivasan, *J. Phys.: Condens. Matter* **20**, 355003 (2008).

<sup>12</sup>Y. Q. Chang, X. Y. Xu, X. H. Luo, C. P. Chen, and D. P. Yu, *J. Cryst. Growth* **264**, 232 (2004).

<sup>13</sup>J. B. Goodenough, *Magnetism and the Chemical Bond* (Wiley, New York, 1963).

<sup>14</sup>M. Sakai, A. Masuno, D. Kan, M. Hashisaka, K. Takata, M. Azuma, M. Takano, and Y. Shimakawa, *Appl. Phys. Lett.* **90**, 072903 (2007).